**Article:**
Zhang, H, Yang, Z, Zhang, X et al. (1 more author) (2014) Photocatalytic effects of wool fibers modified with solely TiO2 nanoparticles and N-doped TiO2 nanoparticles by using hydrothermal method. Chemical Engineering Journal, 254 (10). pp. 106-114. ISSN 1385-8947

https://doi.org/10.1016/j.cej.2014.05.097

This is a post-refereeing final draft. When citing, please refer to the published version: H Zhang, Z Yang, X Zhang and N Mao (2014). Photocatalytic effects of wool fibers modified with solely TiO2 nanoparticles and N-doped TiO2 nanoparticles by using hydrothermal method, Chemical Engineering Journal, Volume 254, 15 October 2014, Pages 106–114
DOI: 10.1016/j.cej.2014.05.097

# Photocatalytic Effects of Wool Fibers Modified with Solely $TiO_2$ Nanoparticles and N-doped $TiO_2$ Nanoparticles by Using Hydrothermal Method

Hui Zhang[*1], Zhenwei Yang[1], Xingtao Zhang[1], and Ningtao Mao[1,2]

[1]School of Textile & Materials, Xi′an Polytechnic University, Xi′an 710048, China

[2]School of Design, University of Leeds, Leeds, LS2 9JT, United Kingdom

[*]Corresponding author: Hui Zhang, School of Textile & Materials, Xi′an Polytechnic University, Xi'an City, Shannxi Province, China

E-mail: hzhangw532@xpu.edu.cn; hzhangw532@163.com

Phone: 0086 029 13002929736

Fax: 0086 029 82330365

**Abstract:** The surfaces of wool fibers are modified with N-doped $TiO_2$ nanoparticles by treating the fibers with tetrabutyl titanate and ammonium chloride under low temperature hydrothermal conditions to obtain wool fibers with photocatalytic functions in the visible light spectrum. The effects of nitrogen and sulfur in amino acids in keratin on the photocatalytic activity of $TiO_2$ particle coated wool fibers are investigated. Changes of various fiber properties such as tensile strength, surface friction, photocatalytic activity, and self-cleaning performance of untreated, $TiO_2$-coated and N-doped $TiO_2$-coated wool fibers are studied. It is found that N-doped anatase $TiO_2$ nanoparticles with an average grain size of 11.2 nm are synthesized and simultaneously grafted onto the wool fibers. After treatments, the crystallization index of the wool fibers is slightly reduced. The capability to protect against ultraviolet radiation is much enhanced. The performances of photocatalytic degradation of methylene blue dye and self-cleaning of red wine under both UV and visible light irradiation are endowed. It is also found that wool fibers coated with $TiO_2$ particles without being doped by nitrogen still have apparent photocatalytic reactions and self-cleaning effects under visible light irradiation due to the formation of C-$Ti^{3+}$, O-$Ti^{3+}$, and N-$Ti^{3+}$ bonds between $TiO_2$ and wool keratin on the wool fiber surfaces. Thus wool fabrics might not need to be coated with N-doped $TiO_2$ nanoparticles to realize its self-cleaning effect under visible light. Such important conclusions would provide wool materials with wide applications in clothing and

technical products such as wastewater treatment.

**Keywords:** Wool fibers; N-doped $TiO_2$, Hydrothermal; Modification

## 1. Introduction

Titanium dioxide ($TiO_2$) loaded textile structures are very attractive not only in functional clothing and home textiles, but also in technical textile applications. One of the typical potential applications of $TiO_2$ loaded textile structure in technical textiles might be its use in the treatment of pollution effluents. While photocatalytic mineralization of organic pollutants by using photocatalyst $TiO_2$ particles is effective to reduce water and air pollutions, the post-treatment removal of $TiO_2$ in either wastewater slurries or air effluent through filtration and re-suspension processes can be a time consuming and costly process [1, 2]. The solution of this problem is to immobilize photocatalyst $TiO_2$ particles on a porous substrate such as fibrous structures, to facilitate the practical application of the photocatalytic wastewater treatment process [3]. Wool fibers are of particular interests in both functional clothing and wastewater treatment substrates. On one hand, wool clothing is notorious for its dimensional stability after scouring and many efforts are made in achieving easy-care wool fabrics, and thus a $TiO_2$ treated and scouring-free wool fabric is long desired. On the other hand, wool fibers are proved an effective keratin substrate to absorb and adsorb organic pollutants and heavy metal ions from waste effluents. Therefore, a visible-light-induced self-decontamination wool fabric has become our research interests.

However, the photocatalytic activities of the $TiO_2$ nanoparticles treated fabrics mentioned above only function in UV light but not in the visible light spectrum. There are two routes to

expand the photocatalytic activities of the $TiO_2$ nanoparticles into visible light spectrum. One is to lower the unoccupied molecular orbital level of the conduction band by ion implantation of metallic elements into $TiO_2$ nanoparticles and the other is to raise the occupied molecular orbital level of the valence band (usually by using organic photosynthesizing dyes or pigments) [4]. The photosynthesizing dyes have the capability of absorbing photons from visible light in a conventional $TiO_2$ thin film, and then transfer them to $TiO_2$, thus creating electricity [5].

Pelaez et al. [6] and Daghrir et al. [7] have systematically reviewed the development of the visible light active $TiO_2$ synthesized by different strategies, including non metal doping (boron, nitrogen, carbon, fluorine, sulfur, etc), noble metal and transition metal doping, dye sensitization, and coupling semiconductors. However, only modest progress in increasing the photocatalytic activity have been made from those efforts because the increased absorption of visible light cannot be straightforwardly related to the reaction rate and the foreign species often work as recombination centers for the photogenerated electron/hole pairs [8].

When doping of $TiO_2$ with nitrogen, the origin of the photoresponse at higher wavelengths is the mixing of the 2p nitrogen level with the oxygen 2p orbital to form the valence band, which results in a lower band gap resulting in visible light absorption [9]. The element nitrogen can be easily incorporated into the $TiO_2$ structure either in the bulk or as a surface dopant because of its comparable atomic size with oxygen, small ionization energy, and high stability [10]. PL analysis confirms that nitrogen atoms in substitutional sites enhance the photocatalysis of $TiO_2$ under visible light more effectively than nitrogen atoms in interstitial sites [11]. Substitution of N in place of oxygen in the $TiO_2$ lattice causes a decrease in oxygen vacancies which inhibits the recombination of electron–hole pairs [12]. However, N doping of $TiO_2$ can enhance the

formation of surface oxygen vacancies [13]. The orbit of doped nitrogen is not responsible for modifying the electron structure of $TiO_2$ but some local unusual structures forming when the N-doping process generates the visible-light activity, such as crystal defects or distortion [14].

Nitrogen and other elements co-doped $TiO_2$ have also been widely investigated. In nitrogen co-doped $TiO_2$, the interstitial nitrogen doping sites rather than substitutional sites seem to improve the photocatalytic activity of $TiO_2$ because of the better charge separation [15]. Moreover, the synergic effect of substitutional and interstitial nitrogen sites are more efficient to improve the electrochemical photoactivity of $TiO_2$ due to the good light absorption, charge transfer in substitutional doping, and the good charge separation induced by the interstitial nitrogen doping [16]. Results indicate that the increased photocatalytic activity of the V-N co-doped $TiO_2$ can be attributed to the synergistic effects caused by V and N that increase the visible light absorption and simultaneously act as electron and hole trapping sites thus decreasing the rate of charge recombination [17]. The visible light photocatalytic activity of N-S co-doped $TiO_2$ is not only influenced by the value of energy gap, the distribution of impurity state, but also depends on the property of impurity state, the location of Fermi level and the energy in the edge of band gap [18]. Examples to achieve visible light photocatalytic functions in $TiO_2$ coated textile fabrics are also reported. Wool fabrics are treated with citric acid as a cross-linking agent and with $TiO_2$/Ag nanocomposites, in which the lowest unoccupied molecular orbital level of $Ti^{3+}$ is lowered by ion implantation of Ag elements into $TiO_2$ nanoparticles, to achieve superior self-cleaning properties [19]. A significantly improved visible-light-induced self-cleaning effect can be achieved in cotton fabrics by using N-doped $TiO_2$ nanoparticles together with AgI particles coating [3].

Unlike cotton fiber, wool fibers are composed of keratin protein and are often not stable in both UV and visible light irradiation [20]. While surface gratification of $TiO_2$ clusters on wool fibers has been realized mainly by the sol-gel process [21, 22] and nanocrystalline $TiO_2$ is found to act primarily as a UV absorber in dry conditions [20] and as a UV photocatalyst in wet conditions [23], there is hardly any research done to achieve visible-light-induced self-cleaning effect in wool fabrics and little is known if nitrogen or sulfur element in amino acids of keratin wool fibers would affect such visible-light-induced photochemical reactions in $TiO_2$ coated wool fibers. In addition, $TiO_2$ nanoparticles are required to be securely bound into the surface of targeted wool fibers in order to increase the durability of the desired photochemical properties and not to release nanoparticles into surrounding environment to meet ecological requirements, also the mechanical properties of the wool fibers need to be maintained.

In this study, wool fibers coated with nitrogen doped $TiO_2$ nanoparticles are achieved by using tetrabutyl titanate as the precursor and ammonium chloride as the doping agent under low temperature hydrothermal conditions, in order to increase its photocatalytic activity of $TiO_2$ nanoparticles under visible light irradiation. The functions of N-doped $TiO_2$ particles and pure $TiO_2$ particles coated wool fibers are compared with each other to find out if nitrogen or sulfur element in amino acids in wool fibers would play a role in self-cleaning effect in $TiO_2$ coated wool fibers. The differences between the tensile properties, friction coefficient, photocatalytic activity, and self-cleaning capability of both pure $TiO_2$ particles and N-doped $TiO_2$ particles coated wool fibers are investigated. The changes of the surface morphology, phase structure, chemical structure, composition, thermal behavior, and optical properties of

the wool fibers before and after treatments are investigated to establish an understanding of the photochemistry mechanism of $TiO_2$ treated wool fibers.

## 2. Experimental section

### 2.1. Materials

The merino wool fibers with an average diameter of 20 μm and nonionic surfactant W900 were obtained from the local textile mill. The reagent-grade chemicals used include tetrabutyl titanate ($Ti(OC_4H_9)_4$), ammonium chloride ($NH_4Cl$), methylene blue (MB), acetone, and anhydrous ethanol. Deionized water was used throughout this study.

### 2.2. Modification of wool fibers with $TiO_2$ and N-doped $TiO_2$ nanoparticles

About 3.0 g of wool fibers was immersed in 200 ml of mixed solution containing 2.0 g/l of sodium carbonate and 0.5% of nonionic surfactant W900 at 50°C for 15 min, and subsequently treated with a 100 ml of acetone and anhydrous ethanol solution at 50°C for 10 min, respectively, and then washed thrice in deionized water at room temperature for 10 min and dried at 60°C for 8 h. About 0.5 ml of tetrabutyl titanate was added dropwise into 10 ml of ethanol solution under vigorous stirring at room temperature. The solution was then diluted with 70 ml of deionized water and 8.0 g of ammonium chloride was added into. About 0.5 g of pretreated wool fibers were dipped in the above suspension for 10 min, and then transferred to a 100 ml PTFE-lined stainless steel autoclave. Six same autoclaves were simultaneously prepared according to the above method, which were placed in a furnace and run at a speed of 10 r/min. The temperature was raised to 110°C at a heating rate of 2.0°C/min. After 2 h, the as-prepared wool fibers were taken out and successively washed with acetone, anhydrous

ethanol, and deionized water at 50°C for 10 min, respectively, and finally dried at 60°C. The resultant precipitate was centrifuged after discarding the upper solution, and successively washed with acetone, anhydrous ethanol, and deionized water, and finally dried in an oven at 120°C for 10 h. For comparative analysis, the wool fibers were also treated with $Ti(OC_4H_9)_4$ without $NH_4Cl$ based on the above described procedure.

**2.3. Characterization and measurement**

The morphology, structure, composition, thermal behavior, and optical properties of the wool fiber samples before and after treatments were characterized by using field emission scanning electron microscopy (FESEM), X-ray diffraction (XRD), Fourier transform infrared spectroscopy (FT-IR), X-ray photoelectron spectroscopy (XPS), thermal gravimetric (TG) analysis, differential scanning calorimetry (DSC), diffuse reflectance spectroscopy (DRS), and photoluminescence (PL) spectroscopy techniques, respectively. The fiber tensile properties were tested by using a standard electromechanical apparatus. The fiber surface friction properties were measured by using a standard single fiber friction measurement device. The photocatalytic activity was performed by monitoring the discoloration of MB dye. The details of the above characterization methods are provided in the Supporting Information S1 of this paper.

The self-cleaning performance of the wool fiber samples was assessed by the discoloration of red wine. A bunch of wool fibers was tied onto a slide glass and about 2 ml of red wine was dropped onto one end of wool padding. After 3 min of absorption of red wine, the wool padding was irradiated with a 1500W Xenon arc lamp which produces UV and visible light irradiation at a distance of 10 cm. The intensities are 5.4 $mW \cdot cm^{-2}$ for UV irradiation and

$1.55\times10^5$ lux for visible light irradiation, respectively. The color changes of the red wine absorbed into the wool padding were monitored by comparing the images taken before and after 84 h of irradiation by using a Samsung ST700 digital camera.

## 3. Results and discussion

$TiO_2$ particles have been used as a delustrant and UV blocker in synthetic fibers for years due to its good reflective properties and UV absorption ability. But in wool fibers, there is possibilities for reactive oxygen species (superoxide radical anions $O_2^{\cdot-}$, hydroxyl radicals ·OH, and hydrogen peroxide) forming by the interaction between UV radiation and $TiO_2$ in the surface of wool fibers to ultimately degrade disulfide bond and produce unwanted yellow photoproducts. In this section, the morphology, chemistry composition, and surface properties of wool fibers coated with $TiO_2$ and N-doped $TiO_2$ nanoparticles in hydrothermal process are examined and discussed.

### 3.1. Tensile properties

The results of the tensile testing of the untreated, $TiO_2$ coated and N-doped $TiO_2$ coated wool fibers before and after irradiation are listed in the Supporting Information S2 (see Table S1). It is found that after treatment with $Ti(OC_4H_9)_4$, the average tenacity and elongation of wool fibers decrease slightly from 219 MPa to 200 MPa and from 25.5% to 22.3%, respectively. After being added with $NH_4Cl$, the average tenacity has almost no further change (202 MPa) and the average elongation increases slightly (25.0%). This seems that the detrimental effect on the tensile properties of wool fibers is due to the hot and high pressure water together with chemical agents.

It is also noticed that, with the increases of the irradiation time, the average tenacity and elongation of the untreated wool fibers gradually decrease. After 500 h of continuous irradiation, the average tenacity and elongation decrease by 13.7% and 25.6%, respectively. However, for both $TiO_2$ coated and N-doped $TiO_2$ coated wool fibers, the average tenacity decreases with the increase of the irradiation time at first, and then levels off beyond 250 h. The average elongation gradually decreases with increasing irradiation time. The average tenacity decreases about 17% for the $TiO_2$ coated and N-doped $TiO_2$ coated wool fibers after being irradiated for 500 h. The decrease of the average elongation of the $TiO_2$ coated wool fibers (43%) is greater than that of the N-doped $TiO_2$ coated wool fibers (39%). Therefore, it is evident that $TiO_2$ coating on wool regardless of N-doped will accelerate the photo-degradation process of wool fibers to some degree. Besides the photodegradation of wool fibers, it is guessed that the increased light absorption of the $TiO_2$ coated and N-doped $TiO_2$ coated wool fibers generates the electron-hole pairs and further forms the active groups [8], which can destroy the structure of wool fibers under UV and visible light irradiation. This is a very interesting phenomenon that $TiO_2$ coated wool fibers have the similar photocatalytic reaction to that of N-doped $TiO_2$ under UV and visible light irradiation. However, because there is not much decrease of wool tensile strength, the photocatalytic reaction site is probably limited to the surface layer of wool fibers. The mechanism of action will be studied in the future work.

### 3.2. Friction properties

The results of the friction testing of the wool fibers before and after treatments are listed in the Supporting Information S3 (see Table S2). After treatment with $Ti(OC_4H_9)_4$ and $NH_4Cl$, as the N-doped $TiO_2$ nanoparticles are immobilized onto the wool fibers, resulting in the surface

morphological changes of wool fibers (became coarse), the static and dynamic friction coefficients of the wool fibers (against-scale and with-scale) increase to some extent. However, the differential frictional coefficients are reduced from 28.0% to 22.7% for static friction testing and reduced from 12.5% to 11.8% for dynamic friction testing, respectively. Because felting effect of wool fibers are determined by directional frictional effect, the smaller the differential frictional coefficient is, the less felting effect the wool fiber has [41]. It is thus anticipated that the felting phenomenon of the N-doped $TiO_2$ coated wool fibers will be alleviated during wet processing including laundering and scouring owing to a reduction of these frictional difference ($\mu_a - \mu_w$). Compared with the N-doped $TiO_2$ coated wool fibers, the static and dynamic friction coefficients of the $TiO_2$ coated wool fibers change little. Thus the nitrogen doping has no effects on the friction properties of the $TiO_2$ coated wool fibers.

### 3.3. Surface morphology

The FESEM images of the wool fibers before and after treatments are shown in the Supporting Information S4 (see Figure S1). It is seen that the surface of the untreated wool fibers is very clean without any substances on. After being modified with $Ti(OC_4H_9)_4$ and $NH_4Cl$, a thin layer of materials is uniformly coated on the surface of the N-doped $TiO_2$ coated wool fibers. Meanwhile, some large granules in micrometer scale adhere onto the fiber surfaces due to the agglomeration of nanoparticles. As illustrated in the high resolution FESEM image, such nanoscale particles with a diameter around 100 nm are tightly anchored to the substrate of the wool fibers. In addition, there is no distinct difference in the surfaces of the $TiO_2$ coated and N-doped $TiO_2$ coated wool fibers. The high pressure and hot water are believed to have facilitated the binding of colloidal nanoparticles to the wool fibers.

### 3.4. Thermal properties

The TG and DSC curves of wool fibers before and after treatments are shown in Figure 1, and the results of TG analysis of wool fibers are listed in the Supporting Information S5 (see Table S3). It is evident from the TG curves that the onset and endset decomposition temperatures of wool fibers decrease from 263.3°C and 381.0°C to 259.7°C and 370.7°C after being treated with $Ti(OC_4H_9)_4$, respectively. The lost mass increases from 63.3% to 67.0% at a temperature of 550°C. After treatment with $Ti(OC_4H_9)_4$ and $NH_4Cl$, the onset and endset decomposition temperatures of the N-doped $TiO_2$ coated wool fibers decrease to 261.9°C and 372.8°C, respectively. The corresponding lost mass is 70.7%.

It is clear from the DSC curves that the initial endothermic peak increases from 81.2°C in untreated wool fibers to 85.1°C in the $TiO_2$ coated wool fibers, which is ascribed to the removal of surface absorbed water or the residual water molecules caused by $TiO_2$ coating. The major endothermic peak at 277.4°C decreases to 273.9°C. That is attributed to the decomposition of both polypeptide and amino acid as well as the incorporation of $TiO_2$ nanoparticles. The initial endothermic peak of the N-doped $TiO_2$ coated wool fibers further decreases to 80.7°C, whereas its major endothermal peak increases to 296.0°C. Obviously, such change in thermal stability of the N-doped $TiO_2$ coated wool fibers is mainly due to the doping of N into $TiO_2$. Therefore, the hydrothermal treatment has a little effect on the thermal properties of wool fibers.

### 3.5. XRD analysis

The XRD patterns of the wool fibers before and after treatments as well as the remaining particles are shown in Figure 2. The typical diffraction peaks for the untreated, $TiO_2$ coated and

N-doped $TiO_2$ coated fibers are found at around 2θ=9° and 20°, which belong to the characteristic positions of wool fibers. However, the characteristic peaks of $TiO_2$ are not observed in the XRD patterns of both modified wool fibers. This might be because the amount of $TiO_2$ nanoparticles loaded onto the fiber surfaces is relatively small so that its diffraction to X-ray cannot be detected by the instrument. The crystallization indexes of wool fibers are reduced from 59.8% to 51.7% for the $TiO_2$ coated wool fibers and 57.3% for the N-doped $TiO_2$ coated wool fibers under hydrothermal conditions, respectively. This might be attributed to the structural change of microfibrils in wool surface. For both the remaining particles left in the hydrothermal processing medium, a series of characteristic peaks at 25°(101), 38°(004), 48°(200), 54°(105), 56°(211), 63°(204), 68°(116), 70°(220) and 75°(215) are in agreement with the data list in JCPDS card No.21-1272 [24]. At the same time, three diffraction peaks are identified at 2θ of 23°, 32°, and 58° in the XRD pattern of the N-doped $TiO_2$ particles, which are attributed to the (100), (110), and (211) planes of salammoniac (JCPDS card No.07-0007). Therefore, the crystalline structure of the as-synthesized particles by using $Ti(OC_4H_9)_4$ and $NH_4Cl$ can be indexed to the anatase $TiO_2$ doped with nitrogen. The average crystallite sizes of the remaining particles in the processing liquid are determined to be 9.6 nm for the $TiO_2$ particles and 11.2 nm for the N-doped $TiO_2$ particles by measuring the FWHM of (101), (004), and (200) reflections and using Scherrer's equation, respectively. Combined with the FESEM observation, the cluster of 100 nm particles is mainly caused by growth of the smaller particles near the surface of wool fibers due to the continuous deposition of small particles.

### 3.6. FT-IR analysis

The FT-IR spectra of the wool fibers before and after treatments as well as the as-obtained

nanoparticles are shown in Figure 3. Compared with the spectrum of the untreated wool fibers, the O-H band of the $TiO_2$ coated wool fibers shifts from 3425 to 3443 $cm^{-1}$. This is ascribed to the surface absorbed water induced by the $TiO_2$ coating [25], which might make the $TiO_2$ coated fiber generate much stronger oxidative free radicals than those of untreated one [26]. The peak at 2932 $cm^{-1}$ ($CH_2$ asymmetric stretching) decreases to 2929 $cm^{-1}$, while the band at 1450 ($CH_3$ asymmetric bending) increases to 1452 $cm^{-1}$. The amide I and III bands shift from 1636 (C=O stretching) and 1234 $cm^{-1}$ (C-N stretching) to 1638 and 1236 $cm^{-1}$, respectively. Furthermore, influenced by the Ti-O band at 462 $cm^{-1}$ of $TiO_2$, the N-H band at 568 increases to 588 $cm^{-1}$ [27].

For the N-doped $TiO_2$ coated wool fibers, the peak at 3430 $cm^{-1}$ is intensified because of the introduction of N-H band. The amide I and III bands decrease to 1628 and 1229 $cm^{-1}$. The peaks at 2932, 2877 ($CH_3$ symmetric stretching), 1708 (carbonyl group), 1450, 933 (C-O stretching), and 568 $cm^{-1}$ shift to 2926, 2875, 1717, 1445, 937, and 578 (influenced by the Ti-O band at 582 $cm^{-1}$ of N-doped $TiO_2$) $cm^{-1}$, respectively. Therefore, it can be concluded that the $TiO_2$ and N-dope $TiO_2$ nanoparticles are immobilized onto the wool fibers by chemical grafting.

### 3.7. XPS analysis

To study the bonding mechanism between $TiO_2$ nanoparticles and wool fibers, the survey spectra and core level single spectra of the bonding partners ($C_{1s}$, $O_{1s}$, $S_{2p}$, $N_{1s}$, and $Ti_{2p}$) of the wool fibers before and after treatments are shown in the Supporting Information S6 (see Figure S2). The quantitative XPS data are listed in the Supporting Information S7 (see Table S4).

It is noticed that the element of titanium appears in the $TiO_2$ coated and N-doped $TiO_2$

coated wool fibers, while it is a much smaller intensity peak in $Ti_{2p}$ in N-doped $TiO_2$ coated wool fibers than in $TiO_2$ coated wool fibers. The percentage atomic concentration of $Ti_{2p}$ in N-doped $TiO_2$ coated wool fibers is about 16% of that in $TiO_2$ coated wool fibers, which indicates a small amount of $TiO_2$ is coated in the N-doped $TiO_2$ coated wool fibers. Also, In comparison with $TiO_2$ coated wool fibers, there are much greater intensity peaks appearing in both $N_{1s}$ and $C_{1s}$ binding energy band in N-doped $TiO_2$ coated wool fibers, and the percentage atomic concentrations of both of these two elements are very close to those of untreated wool fibers as shown in Table S4.

Compared with the $C_{1s}$ XPS spectra of the untreated wool fibers, the sub-peaks of C-C/C-H, C-N/C-O, and C=O/C(O)N of the $TiO_2$ coated fibers shift from 284.54, 286.23, and 287.61 eV to 284.60, 285.89, and 287.77 eV, respectively. A new sub-peak at the binding energy of 283.47 (C-$Ti^{4+}$/C-$Ti^{3+}$) eV is observed [28]. For the N-doped $TiO_2$ coated fibers, the sub-peaks of C-C/C-H, C-N/C-O, and C=O/C(O)N shift to 284.39, 285.90, and 287.78 eV, respectively [29, 30]. Meanwhile, two new sub-peaks at the binding energies of 280.08 (C-$Ti^{3+}$) and 282.37 (C-$Ti^{4+}$) eV are identified [31]. These are attributed to C atoms of wool fibers bound to Ti of N-doped $TiO_2$.

The $O_{1s}$ peak of the untreated wool fibers is deconvoluted into two subpeaks. After treatment with $Ti(OC_4H_9)_4$, the subpeaks at 531.42 (O=C) and 532.39 (O-C) eV shift to 531.80 and 533.50 eV, respectively. Moreover, two new subpeaks are found. The subpeak at 530.44 eV is assigned to O atoms bound to Ti of $TiO_2$ (O-$Ti^{4+}$). The subpeak at 528.73 eV is ascribed to O atoms of wool fibers bound to Ti of $TiO_2$ (O-$Ti^{3+}$). After being modified with $Ti(OC_4H_9)_4$ and $NH_4Cl$, the subpeaks at 531.42 and 532.39 eV shift to 531.09 and 532.54 eV, respectively.

Also, two new subpeaks are identified. The subpeak at 529.16 eV is attributed to O atoms bound to Ti of N-doped $TiO_2$ (O-$Ti^{4+}$) [32]. The subpeak at 526.88 eV is assigned to O atoms of wool fibers bound to Ti of N-doped $TiO_2$ (O-$Ti^{3+}$) [33].

With respect to the $S_{2p}$ XPS spectra of the untreated wool fibers, the subpeaks at 163.42 (S-S) and 164.67 (S-H) eV change little (163.21 and 164.75 eV) when wool fibers are modified with $Ti(OC_4H_9)_4$. After treatment with $Ti(OC_4H_9)_4$ and $NH_4Cl$, the subpeaks at 163.42 and 164.67 eV are reduced to 161.90 and 163.87 eV, respectively. Furthermore, a shoulder at lower binding energy of 159.18 eV is noticed. This has been assigned to S atoms of wool fibers bound to Ti of N-doped $TiO_2$ (S-$Ti^{3+}$) [34]. However, it has been reported that the peak of a binding energy between 163–164 eV is assigned to element sulfur or TiS [35], and that $TiS_2$ nanoparticles is fabricated by sol-gel process [36, 37], therefore, there might be the new bindings of S-$Ti^{4+}$, S-$Ti^{3+}$, and S-$Ti^{2+}$ forming between wool fibers and $TiO_2$ nanoparticles in the hydrothermal process.

For the $N_{1s}$ XPS spectra of three wool fiber samples, the subpeaks at 398.62 (C-N) and 400.08 (N-H) eV in untreated wool fibers slightly shift to 398.77 and 400.10 eV after treatment with $Ti(OC_4H_9)_4$, respectively. A small subpeak at 396.86 eV also forms in the wool fibers treated with $Ti(OC_4H_9)_4$, and this new subpeak is ascribed to the bonding of nitrogen atoms of wool fibers with Ti of $TiO_2$ [38]. This means that the N atoms of wool fibers are bound to Ti of N-doped $TiO_2$ (N-$Ti^{4+}$/N-$Ti^{3+}$). When wool fibers are treated with $Ti(OC_4H_9)_4$ and $NH_4Cl$, the subpeaks at 398.62 and 400.08 eV are reduced to 397.68 and 399.69 eV, respectively. Meanwhile, a new subpeak at 395.12 eV is found, which can be attributed to the nitrogen replacing the oxygen in the crystal lattice of N-doped $TiO_2$ [39, 40]. Thus those characteristics

of $C_{1s}$, $S_{2p}$, and $N_{1s}$ in N-doped $TiO_2$ coated wool fibers are not the same as those of $TiO_2$ coated wool fibers.

The $Ti_{2p}$ XPS spectra for both modified wool fibers consist of four distinct subpeaks. For the $TiO_2$ coated wool fibers, the subpeaks at 464.48 and 459.28 eV represent C-$Ti^{4+}$/O-$Ti^{4+}$/N-$Ti^{4+}{}_{2p1/2}$ and C-$Ti^{4+}$/O-$Ti^{4+}$/N-$Ti^{4+}{}_{2p3/2}$, respectively [14]. The subpeaks at 462.73 and 457.60 eV correspond to C-$Ti^{3+}$/O-$Ti^{3+}$/N-$Ti^{3+}{}_{2p1/2}$ and C-$Ti^{3+}$/O-$Ti^{3+}$/N-$Ti^{3+}{}_{2p3/2}$ respectively. But for the N-doped $TiO_2$ coated wool fibers, the subpeaks at 464.85 and 458.80 eV are in accord with C-$Ti^{4+}$/O-$Ti^{4+}$/S-$Ti^{4+}$/N-$Ti^{4+}{}_{2p1/2}$ and C-$Ti^{4+}$/O-$Ti^{4+}$/S-$Ti^{4+}$/N-$Ti^{4+}{}_{2p3/2}$, respectively. The subpeaks at 462.77 and 456.51 eV agree with C-$Ti^{3+}$/O-$Ti^{3+}$/S-$Ti^{3+}$/N-$Ti^{3+}{}_{2p1/2}$ and C-$Ti^{3+}$/O-$Ti^{3+}$/S-$Ti^{3+}$/N-$Ti^{3+}{}_{2p3/2}$, respectively. Therefore, the results testify that the N-doped $TiO_2$ nanoparticles are grafted onto the wool fibers via the C-$Ti^{4+}$($Ti^{3+}$), O-$Ti^{4+}$($Ti^{3+}$), S-$Ti^{4+}$($Ti^{3+}$, $Ti^{2+}$), and N-$Ti^{4+}$($Ti^{3+}$) bonds.

While it is known that titanium trivalent ($Ti^{3+}$) on the surface of $TiO_2$ particles is very reactive [41] and plays an essential role in photocatalytic process over $TiO_2$ photocatalyst [42], and that it can be generated by using UV irradiation and thermal annealing on the surface of anatase $TiO_2$ particles, we thus propose that the stable bonding between $TiO_2$ particles and wool fibers are C-$Ti^{4+}$, S-$Ti^{4+}$($Ti^{2+}$), O-$Ti^{4+}$, and N-$Ti^{4+}$, and the reaction mechanism between $TiO_2$ nanoparticles and wool fibers is summarized in Figure 4.

### 3.8. DRS analysis

The diffuse reflectance spectra of the untreated, $TiO_2$ coated and N-doped $TiO_2$ coated wool fiber samples in the wavelength range of 200-800 nm are shown in Figure 5.

In comparison with untreated wool samples, it is noted that the reflectance of the $TiO_2$

coated fiber samples decreases in the UV region (200nm~400nm) and increases significantly in the visible light region (450nm~800nm); and that such decrease of the reflectance in the UV region in N-doped $TiO_2$ coated wool fiber samples is relatively small but the increase of the reflectance in the visible light region (450nm~800nm) is still significant. This increase of the reflectance in the visible light region is a band gap narrowing effect which might be due to $N_{2p}$ and $S_{2p}$ states mixing with $O_{2p}$ states in N-doped $TiO_2$ coated fibers, as it is known that the substitutional doping of nitrogen into the $TiO_2$ lattice causes a shift of the absorption edge towards the visible spectral region [9]. With the increase of the substitutional nitrogen sites in the $TiO_2$ lattice, the UV activity decreases but not the visible light photoactivity [16]. The photocatalytic activity of the N-doped $TiO_2$ coated wool fibers is thus enhanced in visible region but weakened in UV region because of the N doping.

However, there is hardly any existing theory that can explain why $TiO_2$ coated wool samples (without N-doping) has such a significant decrease of reflectance in UV band and increase in visible light band. We suspect that such decrease of reflectance in UV band is due to the role of existing C, O, and N elements existing in keratin protein, which forms a certain amount of C-$Ti^{3+}$, O-$Ti^{3+}$ and N-$Ti^{3+}$ bands with $TiO_2$ as indicated in XPS analysis and thus promote photocatalytic activities in the $TiO_2$ coated wool fibers [28, 38, 43]. The increase of the reflectance in visible light region is mainly due to the increase of the whiteness of $TiO_2$ coated wool fibers.

It is also shown that, in comparison with the average reflectance of wool fibers coated with pure $TiO_2$, the average reflectance of the wool fibers coated with N-doped $TiO_2$ is about 1.3% smaller in the UV waveband and about 5.0% greater in the visible band. This might be due to

the fact that the amount of $TiO_2$ applied onto wool fibers in N-doped $TiO_2$ coated wool is much smaller than that in pure $TiO_2$ coated wool, as indicated in XPS results.

The effect of such small differences in the average diffuse reflectance on the photocatalysis and self-cleaning performance between $TiO_2$ coated and N-doped $TiO_2$ coated wool fibers will be investigated further in next few sections.

### 3.9. PL analysis

The PL spectra of the wool fibers before and after treatments are shown in the Supporting Information S8 (see Figure S3). It is known that the PL spectrum of $TiO_2$ is related to its transfer behavior of photo-induced electrons and holes ($TiO_6$ octahedra and oxygen vacancies), reflecting the separation and recombination of charge carriers [44]. For the $TiO_2$ coated wool fibers, a broad emission band can be observed in the range of 320–560 nm (direct electron-hole radiative recombination for 320-400 nm, indirect band gap and surface recombination for 400-500 nm, and charge transfer transition of trapped electron in an oxygen vacancy and $Ti^{3+}$ defects for 500-560 nm), which is consistent with the previous studies [45–47]. Although the shape and position of the PL emission peaks are almost identical, the PL intensity of the $TiO_2$ coated wool fibers is lower than those of the N-doped $TiO_2$ coated wool fibers expect for the sample doped with 100g/l of $NH_4Cl$. This is because doping of N into the $TiO_2$ lattice results in the effective quenching of photoluminescence [48].

It is also observed that the PL intensity of the N-doped $TiO_2$ coated wool fibers gradually decreases with the increase of the amount of $NH_4Cl$ at first, and then reaches the lowest value when the amount of $NH_4Cl$ is 100 g/l, indicating the low recombination rate of photogenerated electron–hole pairs and the reduction of surface $Ti^{3+}$ species, which leads to the high

photocatalytic activity [49]. After that, the PL intensity increases with increasing the amount of $NH_4Cl$. This is due to an increase in the formation of vacancy sites, which can increase the probability of charge recombination [50]. As a result, the N-doping level causes the change in the valence band level of N-doped $TiO_2$, which results from the photocatalytic formation of OH· radicals induced by irradiation with visible light.

### 3.10. Photocatalysis

The photocatalytic activity of the untreated, $TiO_2$ coated and N-doped $TiO_2$ coated wool fibers are characterized by measuring the absorbance of MB solution under both UV and visible light irradiation. The change of normalized $C_0/C$ of MB concentration with irradiation time is shown in the Supporting Information S9 (see Figure S4). It is evident that the normalized $C_0/C$ gradually increases with the increase of irradiation time for all samples under both UV and visible light irradiation.

While the UV rays can decolorize the MB dye to some degree due to UV photo-bleaching [51], it is found in Figure S4(a) that, the $TiO_2$ coated wool fibers behave much better than the N-doped $TiO_2$ coated ones under UV irradiation condition. The apparent rate constant of the normalized $C_0/C$ for the $TiO_2$ coated wool fibers (0.41 $h^{-1}$, squared correlation coefficient, $R^2$=0.96) is as about 1.2 times as that for the N-doped $TiO_2$ coated ones (0.34 $h^{-1}$, $R^2$=0.99). This might be because there is a greater amount of $TiO_2$ particles coated on the surface of wool fibers. After being irradiated by visible light irradiation for a specific time, it appears in Figure S4(b) that the apparent rate constant of the normalized $C_0/C$ of the N-doped $TiO_2$ coated wool fibers (0.15 $h^{-1}$, $R^2$=0.93) is as about 1.15 times as that of the $TiO_2$ coated fibers (0.13 $h^{-1}$, $R^2$=0.94), although there are much less amount of N-doped $TiO_2$ particles immobilized on wool

samples than the amount of pure $TiO_2$ particles on wool fibers as indicated in XPS results. The visible light activity of the N-doped $TiO_2$ coated wool fibers during the MB degradation process might be attributed to the N- and/or S-induced mid-gap level forming above the valence band of $TiO_2$ [51, 52]. Based on the analyses of XPS, DRS and PL, it is concluded that the nitrogen and sulfur anions act as the hole traps, reducing the recombination rate of the hole–electron couples [53]. Moreover, the oxygen deficient sites forming in the grain boundaries are responsible for the visible light response [54], whilst the presences of nitrogen and sulfur improve the stabilization of these oxygen vacancies [55, 56].

### 3.11. Self-cleaning performance under the mixture of UV and visible lights

The images of the untreated, $TiO_2$ coated and N-doped $TiO_2$ coated wool fibers stained by red wine before and after irradiation are shown in Figure 6. It is interesting to note that the self-cleaning performance of the wool fibers after treatment with $Ti(OC_4H_9)_4$ can be achieved regardless of $NH_4Cl$ being added. After 84 h of UV and visible light irradiation, the intensity of the red color on the untreated wool padding stained by red wine still remains intact. However, the red color on the surface of the $TiO_2$ coated wool padding is almost completely discolored while the red color of N-doped $TiO_2$ coated wool padding can still be seen. When exposed to UV and visible light irradiation, a photon with energy greater than the band gap of $TiO_2$ generates an electron hole pair. The positive hole in the valence band can react with the absorbed water to produce $H^+$ and ·OH radicals, and the electron in the conduction band can reduce oxygen to produce $O_2^{\cdot -}$ anions. Both hydroxyl radicals and peroxide anions are extremely reactive species, and they can oxidize the organic compounds of red wine until complete mineralization is achieved [57]. It is confirmed that by merging with a subsurface

oxygen vacancies ($V_O$), $O_2$ adsorbed as superoxo ($O_2^-$) at fivefold-coordinated Ti sites can be transformed to peroxo ($O_2^{2-}$) and placed into an anion surface lattice site as an interstitial $(O_2)_O$ species, which is also an important intermediate in the photooxidation of water [58]. The photocatalytic activity of the N-doped $TiO_2$ coated wool fibers can be enhanced in visible region because of the N doping, but weakened in UV region. In addition, it is noticed that the introduction of $NH_4Cl$ into hydrothermal process reduces the amount of $TiO_2$ particles forming on the surface of wool fibers and thus reduces the total photocatalytic activity of the N-doped $TiO_2$ coated wool fibers under UV and visible light irradiation. In contrast, the wool fibers after treatment solely with $Ti(OC_4H_9)_4$ have much greater amount of $TiO_2$ particles coated on the surface of wool and also have C-$Ti^{3+}$ and N-$Ti^{3+}$ bonds forming on the surface of the wool fiber and could thus have photocatalytic activities under both UV and visible light irradiation. Therefore, the self-cleaning ability of the $TiO_2$ coated wool fibers is much better than that of the N-doped $TiO_2$ coated ones under a combination of UV and visible light irradiation.

## 4. Conclusions

The N-doped $TiO_2$ nanoparticles have been prepared by using tetrabutyl titanate as the precursor and ammonium chloride as the doping agent in the presence of wool fibers under hydrothermal conditions. The photocatalytic effects have been compared with the wool fibers treated solely using tetrabutyl titanate as the precursor under similar hydrothermal conditions. The SEM and XRD results confirm that the surfaces of the wool fibers are coated with a thin film of anatase-type N-doped $TiO_2$ nanoparticles with an average nanocrystal size of 11.2 nm. The FT-IR and XPS results confirm that the N-doped $TiO_2$ nanoparticles are grafted onto the

wool fibers through the chemical bonds of C-$Ti^{4+}$, S-$Ti^{4+}$($Ti^{2+}$), and N-$Ti^{4+}$. There are also N- and S-$Ti^{3+}$ bonds forming between $TiO_2$ particles and the surface of wool fibers, which enable the photocatalytic activities of $TiO_2$ nanoparticles under visible light irradiation. The TG and DSC results confirm that the thermal properties of wool fibers have only small changes. The coefficients of friction increase, while the differential frictional coefficients decrease. The DRS, PL and tensile results confirm that there are photocatalytic activities and photodegradation reactions happening in the $TiO_2$ coated and N-doped $TiO_2$ coated wool fibers. A certain amount of N-dopant incorporated into $TiO_2$ accelerates the evolution of $O_2$. The self-cleaning performances confirm that wool keratin polymers could form C-, N-, and O-$Ti^{3+}$ bonding with $TiO_2$ particles to have photocatalysis effect and self-cleaning performance under visible light irradiation.

**Acknowledgement**

The authors are grateful for the supporting fund from the Education Department of Shaanxi Province of China (Grant No.12JK0564). The corresponding author also acknowledges the Youth Leading Scholar Supporting Plan of Xi'an Polytechnic University.

**References**

[1] J. A. Byrne, B. R. Eggins, N. M. D. Brown, B. McKinney, M. Rouse, Immobilisation of

$TiO_2$ Powder for the Treatment of Polluted Water. Appl. Catal. B–Environ, **17** (1998) 25–36.

[2] N. M. Mahmoodia, M. Arami, N. M. Mahmoodi, M. Arami, Bulk Phase Degradation of Acid Red 14 by Nanophotocatalysis Using Immobilized Titanium(IV) Oxide Nanoparticles. J. Photochem. Photobiol. A. **182** (2006) 60–66.

[3] D. Wu, M. Long, Realizing Visible-light-induced Self-cleaning Property of Cotton through Coating N-$TiO_2$ Film and Loading AgI Particles. ACS Appl. Mater. Inter. **3** (2011) 4770–4774.

[4] M. A. Henderson, A Surface Science Perspective on $TiO_2$ Photocatalysis. Surf. Sci. Rep. **66** (2011) 185−297.

[5] Y. Li, Z. Y. Fu, B. L. Su, Hierarchically Structured Porous Materials for Energy Conversion and Storage. Adv. Funct. Mater. **22** (2012) 4634–4667.

[6] M. Pelaez, N. T. Nolan, S. C. Pillai, M. K. Seery, P. Falaras, A. G. Kontos, P. S. M. Dunlop, J. W. J. Hamilton, J. A. Byrne, K. O'Shea, M. H. Entezari, D. D. Dionysiou, A Review on the Visible Light Active Titanium Dioxide Photocatalysts for Environmental Applications. Appl. Catal. B–Environ. **125** (2012) 331–349.

[7] R. Daghrir, P. Drogui, D. Robert, Modified $TiO_2$ for Environmental Photocatalytic Applications: A Review. Ind. Eng. Chem. Res. **52** (2013) 3581–3599.

[8] A. Di Paola, E. Garcia-Lopez, G. Marci, L. Palmisano, A Survey of Photocatalytic Materials for Environmental Remediation. J. Hazard. Mater. **211–212** (2012) 3–29.

[9] T. L. Thompson, J. T. Yates, Surface Science Studies of the Photoactivation of $TiO_2$ – New Photochemical Processes. Chem. Rev. **106** (2006) 4428–4453.

[10] D. Wu, M. Long, W. Cai, C. Chen, Y. Wu, Low Temperature Hydrothermal Synthesis of N-doped $TiO_2$ Photocatalyst with High Visible-light Activity. J. Alloys Compd. **502** (2010)

289–294.

[11] S. Lee, I. S. Cho, D. K. Lee, D. W. Kim, T. H. Noh, C. H. Kwak, S. Park, K. S. Hong, J. K. Lee, H. S. Jung, Influence of Nitrogen Chemical States on Photocatalytic Activities of Nitrogen-doped $TiO_2$ Nanoparticles under Visible Light. J. Photochem. Photobiol. A. **213** (2010) 129–135.

[12] K. Selvam, M. Swaminathan, Nano N-$TiO_2$ Mediated Selective Photocatalytic Synthesis of Quinaldines from Nitrobenzenes. RSC Adv. **2** (2012) 2848–2855.

[13] H. Y. Li, S. L. Zhang, Q. Zhong, Effect of Nitrogen Doping on Oxygen Vacancies of Titanium Dioxide Supported Vanadium Pentoxide for Ammonia-SCR Reaction at Low Temperature. J. Colloid Interf. Sci. **402** (2013) 190–195.

[14] T. Sano, N. Mera, Y. Kanai, C. Nishimoto, S. Tsutsui, T Hirakawa, N. Negishi, Origin of Visible-light Activity of N-doped $TiO_2$ Photocatalyst: Behaviors of N and S Atoms in a Wet N-doping Process. Appl. Catal. B–Environ. **128** (2012) 77–83.

[15] Y. L. Pang, A. Z. Abdullah, Effect of Carbon and Nitrogen Co-doping on Characteristics and Sonocatalytic Activity of $TiO_2$ Nanotubes Catalyst for Degradation of Rhodamine B in Water. Eng. J. **214** (2013) 129–138.

[16] H. Fakhouri, J. Pulpytel, W. Smith, A. Zolfaghari, H. R. Mortaheb, F. Meshkini, R. Jafari, E. Sutter, F. Arefi-Khonsari, Control of the Visible and UV Light Water Splitting and Photocatalysis of Nitrogen Doped $TiO_2$ Thin Films Deposited by Reactive Magnetron Sputtering. Appl. Catal. B–Environ. **144** (2014) 12–21.

[17] R. Jaiswal, N. Patel, D. C. Kothari, A. Miotello, Improved Visible Light Photocatalytic Activity of $TiO_2$ Co-doped with Vanadium and Nitrogen. Appl. Catal. B–Environ. **126** (2012)

47–54.

[18] P. Zhou, J. Yu, Y. Wang, The New Understanding on Photocatalytic Mechanism of Visible-light Response N–S Codoped Anatase $TiO_2$ by First-principles. Appl. Catal. B–Environ. **142–143** (2013) 45–53.

[19] M. Montazer, A. Behzadnia, M. B. Moghadam, Superior Self-cleaning Features on Wool Fabric Using $TiO_2$/Ag Nanocomposite Optimized by Response Surface Methodology. J. Appl. Polym. Sci. **125** (2012) E356–E363.

[20] H. Zhang, K. R. Millington, X. G. Wang, The Photostability of Wool Doped with Photocatalytic Titanium Dioxide Nanoparticles. Polym. Degrad. Stab. **94** (2009) 278–283.

[21] W. A. Daoud, S. K. Leung, W. S. Tung, J. H. Xin, K. Cheuk, K. Qi, Self-cleaning Keratins. Chem. Mater. **20** (2008) 1242–1244.

[22] W. S. Tung, W. A. Daoud, Photocatalytic Formulations for Protein Fibers: Experimental Analysis of the Effect of Preparation on Compatibility and Photocatalytic Activities. J. Colloid Interf. Sci. **32** (2008) 283–288.

[23] M. Montazer, E. Pakdel, Reducing Photo-yellowing of Wool Using Nano $TiO_2$. Photochem. Photobiol. **86** (2010) 255–260.

[24] H. Liu, M. Wang, Y. Wang, Y. Liang, W. Cao, Y. Su, Ionic Liquid-templated Synthesis of Mesoporous $CeO_2$–$TiO_2$ Nanoparticles and Their Enhanced Photocatalytic Activities under UV or Visible Light. J. Photochem. Photobiol. A. **223** (2011) 157–164.

[25] S. H. Hsieh, F. R. Zhang, H. S. Li, Anti-ultraviolet and Physical Properties of Woolen Fabrics Cured with Citric Acid and $TiO_2$/chitosan. J. Appl. Polym. Sci. **100** (2006) 4311–4319.

[26] Q. He, Z. Zhang, J. Xiong, Y. Xiong, H. Xiao, A Novel Biomaterial—$Fe_3O_4$:$TiO_2$

Core-shell Nano Particle with Magnetic Performance and High Visible Light Photocatalytic Activity. Opt. Mater. **31** (2008) 380–384.

[27] M. Ye, Q. Zhang, Y. Hu, J. Ge, Z. Lu, L. He, Z. Chen, Y. Yin, Magnetically Recoverable Core-shell Nanocomposites with Enhanced Photocatalytic Activity. CHEM-EUR J. **16** (2010) 6243–6250.

[28] Y. Huang, W. Ho, S. Lee, L. Zhang, G. Li, J. C. Yu, Effect of Carbon Doping on the Mesoporous Structure of Nanocrystalline Titanium Dioxide and Its Solar-light-driven Photocatalytic Degradation of NOx. Langmuir, **24** (2008) 3510–3516.

[29] R. J. Ward, H. A. Willis, G. A. George, G. B. Guise, R. J. Denning, D. J. Evans, R. D. Short, Surface Analysis of Wool by X-ray Photoelectron Spectroscopy and Static Secondary Ion Mass Spectrometry. Text. Res. J. **63** (1993) 362–368.

[30] B. Kidd, C. M. Carr, K. J. Dodd, J. Vickermanand, K. Byrne, X-ray Photoelectron Spectroscopic Study of Wool Modified by Gaseous Fluorine. Text. Res. J. **65** (1995) 504–506.

[31] S. Atul, The Pearson Guide to Physical Chemistry for the Aipmt, first ed., Pearson Education, India, 2011.

[32] Y. C. Zhang, M. Yang, G. Zhang, D. D. Dionysiou, $HNO_3$-involved One-step Low Temperature Solvothermal Synthesis of N-doped $TiO_2$ Nanocrystals for Efficient Photocatalytic Reduction of Cr(VI) in Water. Appl. Catal. B–Environ. **142–143** (2013) 249–258.

[33] V. V. Atuchin, V. G. Kesler, N. V. Pervukhina, Z. Zhang, Ti 2p and O 1s Core Levels and Chemical Bonding in Titanium-bearing Oxides. J. Electron. Spectrosco. Relat. Phenom., **152** (2006) 18–24.

[34] S. Sune, Atomic and Molecular Spectroscopy: Basic Aspects and Practical Applications, first ed., Springer, Berlin, 2004.

[35] S. N. Dutta, D. Dowerah, D. C. Frost, Study of Sulphur in Assam Coals by X-ray Photoelectron Spectroscopy. Fuel. **62** (1983) 840–841.

[36] S. Sakka, Handbook of Sol-gel Science and Technology: Processing, Characterization and Applications, V. I - Sol-Gel Processing, first ed., Springer, Berlin, 2005.

[37] M. A. Sriram, P. N. Kumta, The Thio-sol-gel Synthesis of Titanium Disulfide and Niobium Disulfide. Part 1.–Materials Chemistry. J. Mater. Chem. **8** (1998) 2441–2451.

[38] M. N. Uddin, S. U. A. Shibly, R. Ovali, S. Islam, M. M. R. Mazumder, M. S. Islam, M. J. Uddin, O. Gulseren, E. Bengu, An Experimental and First-principles Study of the Effect of B/N Doping in $TiO_2$ Thin Films for Visible Light Photo-catalysis. J. Photochem. Photobiol. A. **254** (2013) 25–34.

[39] C. W. H. Dunnill, Z. A. Aiken, J. Pratten, M. Wilson, D. J. Morgan, I. P. Parkin, Enhanced Photocatalytic Activity under Visible Light in N-doped $TiO_2$ Thin Films Produced by APCVD Preparations Using T-butylamine as a Nitrogen Source and Their Potential for Antibacterial Films. J. Photochem. Photobiol. A. **207** (2009) 244–253.

[40] F. Napoli, M. Chiesa, S. Livraghi, E. Giamello, S. Agnoli, G. Granozzi, G. Pacchioni, C. Di Valentin, The Nitrogen Photoactive Centre in N-doped Titanium Dioxide Formed via Interaction of N Atoms with the Solid. Nature and Energy Level of the Species. Chem. Phys. Lett. **477** (2009) 135–138.

[41] A. Sirisuk, E. Klansorn, P. Praserthdam, Effects of Reaction Medium and Crystallite Size on $Ti^{3+}$ Surface Defects in Titanium Dioxide Nanoparticles Prepared by Solvothermal Method.

Catal. Commun. **9** (2008) 1810–1814.

[42] H. Liu, H. T. Ma, X. Z. Li, W. Z. Li, M. Wu, X. H. Bao, The Enhancement of $TiO_2$ Photocatalytic Activity by Hydrogen Thermal Treatment. Chemosphere. **50** (2003) 39–46.

[43] B. Li, Z. Zhao, F. Gao, X. Wang, J. Qiu, Mesoporous Microspheres Composed of Carbon-coated $TiO_2$ Nanocrystals with Exposed {001} Facets for Improved Visible Light Photocatalytic Activity. Appl. Catal. B–Environ. **147** (2014) 958–964.

[44] Z. Q. Liu, Y. C. Wang, W. Chu, Z. H. Li, C. C. Ge, Characteristics of Doped $TiO_2$ Photocatalysts for the Degradation of Methylene Blue Waste Water under Visible Light. J. Alloy. Compd. **501** (2010) 54–59.

[45] X. Liu, Z. Q. Liu, J. Zheng, X. Yan, D. D. Li, S. Chen, W. Chu, Characteristics of N-doped $TiO_2$ Nanotube Arrays by $N_2$-plasma for Visible Light-driven Photocatalysis. J. Alloy. Compd. **509** (2011) 9970– 9976.

[46] X. Xiang, X. Y. Shi, X. L. Gao, F. Ji, Y. J. Wang, C. M. Liu, X. T. Zu, Effect of N-doping on Absorption and Luminescence of Anatase $TiO_2$ Films. Chin. Phys. Lett. **29** (2012) 027801.

[47] Z. Z. Zhang, J. L. Long, X. Q. Xie, H. Lin, Y. G. Zhou, R. S. Yuan, W. X. Dai, Z. X. Ding, X. X. Wang, X. Z. Fu, Probing the Electronic Structure and Photoactivation Process of Nitrogen-doped $TiO_2$ Using DRS, PL, and EPR. ChemPhysChem. **13** (2012) 1542–1550.

[48] L. Gomathi Devi, B. Nagaraj, K. Eraiah Rajashekhar, Synergistic Effect of Ag Deposition and Nitrogen Doping in $TiO_2$ for the Degradation of Phenol under Solar Irradiation in Presence of Electron Acceptor. Chem. Eng. J. **181**–**182** (2012) 259–266.

[49] Y. L. Chen, X. X. Cao, B. Z. Lin, B. F. Gao, Origin of the Visible-light Photoactivity of $NH_3$-treated $TiO_2$: Effect of Nitrogen Doping and Oxygen Vacancies. Appl. Surf. Sci. **264** (2013)

845–852.

[50] H. J. Yun, David M. Lee, S. Yu, J. Yoon, H. J. Park, J. Yi, Effect of Valence Band Energy on the Photocatalytic Performance of N-doped $TiO_2$ for the Production of $O_2$ via the Oxidation of Water by Visible Light. J. Mol. Catal. A–Chem. **377** (2013) 221–226.

[51] M. B. Fisher, D. A. Keane, P. Fernandez-Ibanez, J. Colreavy, S. J. Hinder, K. G. McGuigan, S. C. Pillai, Nitrogen and Copper Doped Solar Light Active $TiO_2$ Photocatalysts for Water Decontamination. Appl. Catal. B–Environ. **130–131** (2013) 8–13.

[52] S. S. Umare, A. Charanpahari, R. Sasikala, Enhanced Visible Light Photocatalytic Activity of Ga, N and S Codoped $TiO_2$ for Degradation of Azo Dye. Mater. Chem. Phys. **140** (2013) 529–534.

[53] M. D. Arienzo, R. Scotti, L. Wahba, C. Battocchio, E. Bemporad, A. Nale, F. Moraz-zoni, Hydrothermal N-doped $TiO_2$: Explaining Photocatalytic Properties by Electronic and Magnetic Identification of N Active Sites. Appl. Catal. B–Environ. **93** (2009) 149–155.

[54] V. Etacheri, M. K. Seery, S. J. Hinder, S. C. Pillai, Oxygen Rich Titania: A Dopant Free, High Temperature Stable, and Visible-light Active Anatase Photocatalyst. Adv. Funct. Mater. **21** (2011) 3744–3752.

[55] T. Ihara, M. Miyoshi, Y. Iriyama, O. Matsumoto, S. Sugihara, Visible-light-active Titanium Oxide Photocatalyst Realized by an Oxygen-deficient Structure and by Nitrogen Doping. Appl. Catal. B-Environ. **42** (2003) 403–409.

[56] K. M. Parida, Nrupara Jsahu, A. K. Tripathi, V. S. Kamble, Gold Promoted S,N-doped $TiO_2$: An Efficient Catalyst for CO Adsorption and Oxidation. Environ. Sci. Technol. **44** (2010) 4155–4160.

[57] Y. L. Kuo, T. L. Su, F. C. Kung, T. J. Wu, A Study of Parameter Setting and Characterization of Visible-light Driven Nitrogen-modified Commercial $TiO_2$ Photocatalysts. J. Hazard. Mater. **190** (2011) 938–944.

[58] M. Setvín, U. Aschauer, P. Scheiber, Y. F. Li, W. Hou, M. Schmid, A. Selloni, U. Diebold, Reaction of $O_2$ with Subsurface Oxygen Vacancies on $TiO_2$ Anatase (101). Science. **341** (2013) 988–991.

**Figure captions:**

**Figure 1**. TG (a) and DSC (b) curves of wool fibers before and after treatments

**Figure 2**. X-ray patterns of wool fibers before and after treatments and the remaining particles

**Figure 3**. FT-IR spectra of wool fibers before and after treatments and the remaining particles

**Figure 4**. Proposed mechanism of wool fiber surface-grafted with N-doped $TiO_2$ nanoparticles

**Figure 5**. DRS of the untreated, $TiO_2$ coated and N-doped $TiO_2$ coated wool fibers

**Figure 6**. The self-cleaning effect of wool fibers before and after 84 h of UV and visible light irradiation: (a) before irradiation; (b) after irradiation

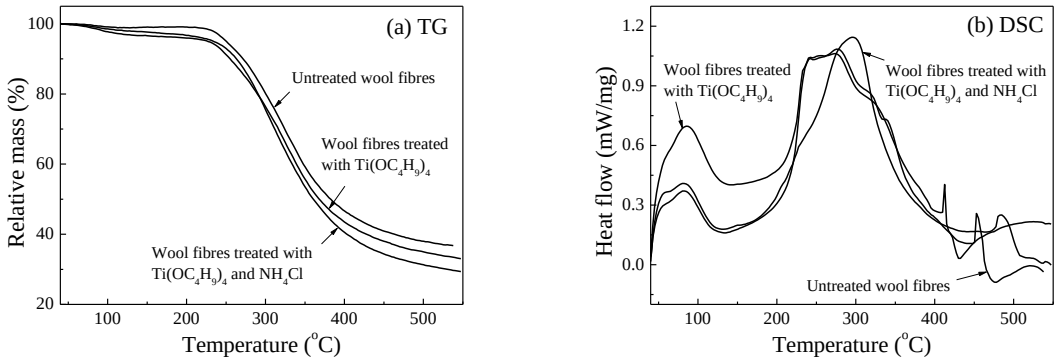


**Figure 1** TG (a) and DSC (b) curves of wool fibres before and after treatments

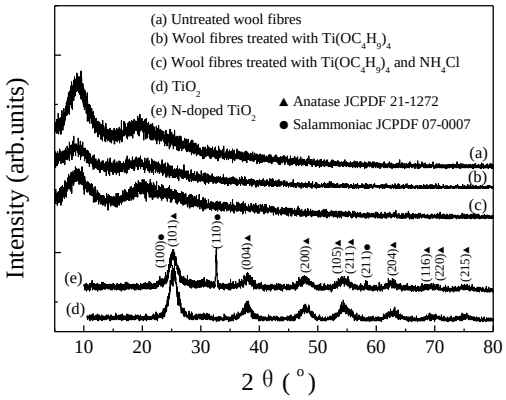


**Figure 2** X-ray patterns of wool fibres before and after treatments and the remaining particles

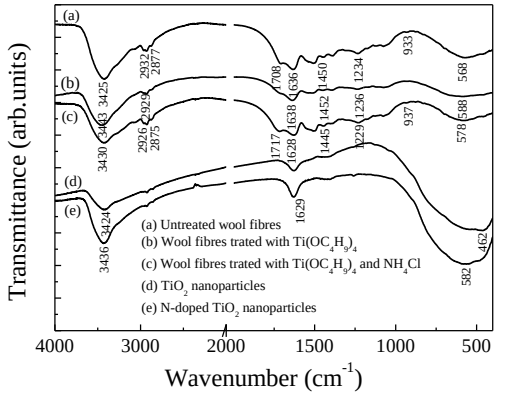


**Figure 3** FT-IR spectra of wool fibres before and after treatments and the remaining particles

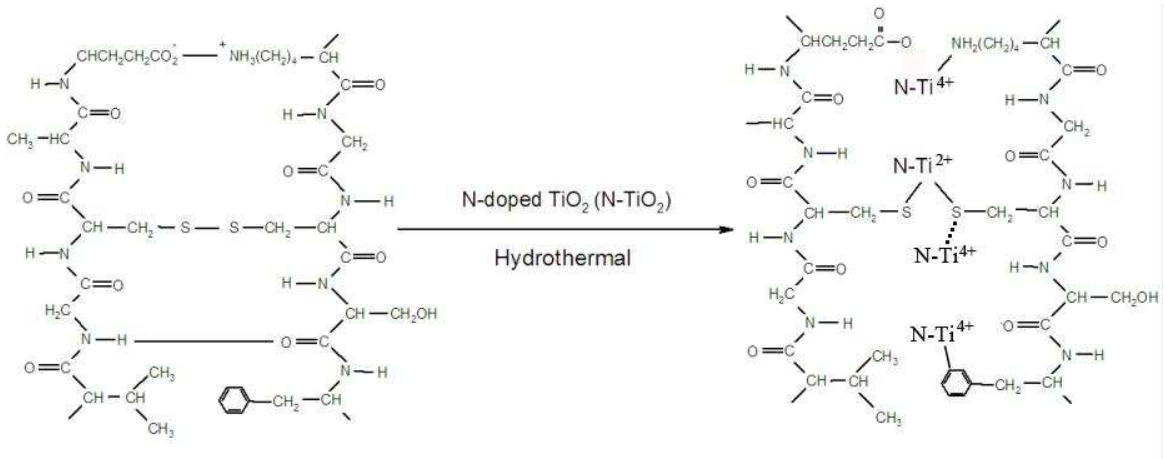


**Figure 4** Proposed mechanism of wool fibre surface-grafted with N-doped $TiO_2$ nanoparticles

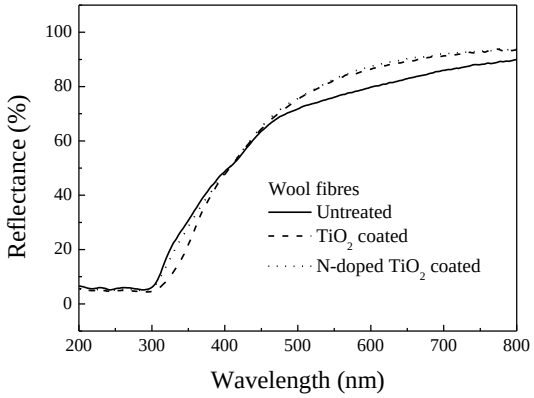


**Figure 5** DRS of the untreated, $TiO_2$ coated and N-doped $TiO_2$ coated wool fibres

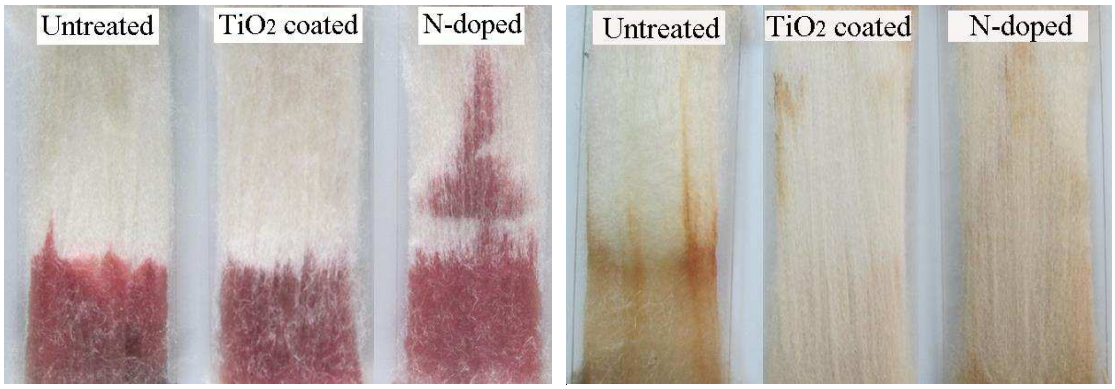


(a) before irradiation (b) after irradiation

**Figure 6** The self-cleaning effect of wool fibres before and after 84 h of UV and visible light irradiation

# Supporting Information

## Photocatalytic Effects of Wool Fibers Modified with Solely $TiO_2$ Nanoparticles and N-doped $TiO_2$ Nanoparticles by Using Hydrothermal Method

Hui Zhang[*1], Zhenwei Yang[1], Xingtao Zhang[1], and Ningtao Mao[1,2]

[1]School of Textile & Materials, Xi'an Polytechnic University, Xi'an 710048, China

[2]School of Design, University of Leeds, Leeds, LS2 9JT, United Kingdom

*To whom correspondence should be addressed. E-mail: hzhangw532@xpu.edu.cn

**S1. Characterization and measurement**

The surface morphologies of the wool fibers before and after treatments were examined by using a field emission scanning electron microscope (FESEM, JEOL JSM-6700).

The X-ray diffraction (XRD) patterns of the fiber samples and as-obtained particles were obtained by using Cu $K\alpha_1$ radiation ($\lambda$=0.154056 nm), with a 7000S diffractometer at 40 kV and 40 mA with an angle of $2\vartheta$ from 5° to 80° at a scan speed of 8 deg/min. The crystallite size of the remaining particles was determined by the Scherrer formula ($D=K\lambda/\beta\cos\theta$, where $D$ is the diameter of the particle; λ is the X-ray wavelength; β is the full width at half maximum (FWHM) of the diffraction line; θ is the diffraction angle; and $K$ is a constant 0.89) [S1]. The crystallization index $CI$ of the fiber samples was calculated by equation 1 [S2].

$$CI = \frac{I_{9^\circ} - I_{14^\circ}}{I_{9^\circ}} \times 100\% \qquad (1)$$

Where $I_{9^\circ}$ and $I_{14^\circ}$ are the intensities of diffraction at 2θ=9° and 2θ=14°, respectively.

Functional groups of untreated and treated wool fibers were analyzed by using Fourier transform Infrared spectroscopy (FT-IR) in an FTIR 7600 spectrophotometer (Lambda Scientific Systems, Inc.). The spectra were recorded in the range of 400–4000 $cm^{-1}$ with a resolution of 4 $cm^{-1}$ as the KBr pellets.

The composition and chemical states of key elements in the fiber surfaces were obtained by using a Thermo Scientific K-Alpha X-ray photoelectron spectrometer (XPS) system. The fiber samples were analyzed with Al Kα monochromatic X-ray source (1486.68 eV, 12 kV, 6 mA) and the vacuum of the analysis chamber was less than $8\times10^{-6}$ Pa. All binding energies were calibrated relative to the $C_{1s}$ peak (284.6 eV) from hydrocarbons absorbed on the surface of the samples. The percentage atomic concentration of component elements were obtained

from XPS peak areas and peak decomposition which were determined using the Thermo Scientific Avantage Data System. The spectrum was first smoothed by using the Savitsky-Golay algorithm (autoapply changes), and the peak background was then processed by using the smart algorithm, and finally the peak was fitted by using the Gauss-Lorentz mixed algorithm.

The changes of the thermal properties of the wool fibers were investigated by using thermogravimetric (TG) and differential scanning calorimetry (DSC) analyses in a NETZSCH STA 449F3 instrument. The percentage weight change and heat flow with respect to temperature were evaluated from 40°C to 550°C with a 10$^{o}$C/min heating rate under a nitrogen atmosphere, respectively. The onset and endset decomposition temperatures and peak decomposition temperature were determined using the attached NETZSCH Proteus Thermal Analysis Software.

The optical properties of the fiber samples were measured by using diffuse reflectance spectroscopy (DRS) in U-3010 spectrophotometer, which was equipped with an integrating sphere (ø150 mm) and barium sulfate ($BaSO_4$). The spectra were recorded at ambient temperature in the 200-800 nm range at a scanning speed of 600 nm/min.

The photoluminescence (PL) spectra of the fiber samples at room temperature were recorded using a Hitachi F-4500 fluorescence spectrophotometer with a 150 W xenon lamp as the light source under photoexcitation at 300 nm.

The photocatalytic degradation of the MB dye in an aqueous solution was performed by using the untreated and treated wool fibers. About 0.4 g of the fiber sample was immersed into 50 ml of a 5 mg/l MB solution, which was placed in a dark box. Every 8 h, the reaction solution was replaced with the same volume of fresh MB solution until the absorbance was

kept at 0.467 at $\lambda_{max}$ 662 nm. The MB solution was then exposed to a Philips 40W UV lamp with a main wavelength of 254 nm at a distance of 10 cm. The intensity of UV irradiation was determined to be 215μW·cm$^{-2}$ by a TM-213 UV illumination meter. To simulate the visible light irradiation, a 125W metal halide lamp was hung over the MB solution at a distance of 15 cm. The solution was covered with a UV filter to block out the UV rays. The intensity of visible light was measured to be 1.25×10$^4$ lux by a TES 1332A digital light intensity meter. The absorbance of the MB solution at $\lambda_{max}$ 662 nm was measured by using a VIS-7220N spectrophotometer (Beijing Rayleigh Analytical Instrument Corp.) at set intervals. The standard curve between the concentration and the absorbance for MB solution was calibrated based on the Beer-Lambert's law. Variation of normalized $C_0/C$ of MB concentration was plotted against irradiation time $t$ and the apparent photo-degradation rate constant $k$ of MB solution was calculated by equation 2 [S3].

$$\ln\frac{C_0}{C} = f(t) = kt \qquad (2)$$

Where $C_0$ is the initial concentration of MB aqueous solution, $C$ is the concentration of MB solution at time $t$.

The wool fibers were irradiated with the aforementioned metal halide lamp at a distance of 15 cm. The room temperature is 26°C and the relatively humidity is 72%. The intensity in visible light waveband is 1.75×10$^4$ lux and the intensity of UV irradiation is 920 μW·cm$^{-2}$. The tensile strength of the fiber samples before and after irradiation was conducted in accordance with GB/T 13835.5-2009 on a YG001N electromechanical measurement device. The gage length was 20 mm and the constant extension rate was 20 mm/min with a pretension of 0.2 cN. More than 300 wool fibers were measured and the average value was recorded.

The changes of the static and dynamic friction coefficients of the wool fibers against a smooth stainless steel rod surface were evaluated based on the capstan method [S4] by using a Y151 single fiber friction measurement device. A defined weight (*W*) was fixed at one end of a single fiber sample and the free end of the single fiber was connected to the hook of a torsion balance, which was hung onto the rod perpendicular to the rotation axis of the rod. The static and dynamic friction coefficients ($\mu_s$ and $\mu_d$) were determined by evaluating the loads imposed on the fiber sample when the cylinder was not rotating and when it was rotating, respectively. The value of either $\mu_s$ or $\mu_d$ was calculated by equation 3 [S5].

$$\mu_s(\mu_d) = 0.733\log W/(W-m) \qquad (3)$$

Where *W* is the initial weight loaded onto one of the ends of fiber sample and *m* is the weight recorded on the torsion balance. The average of 50 tests was calculated. The differential frictional coefficient (static $\sigma_s$ or dynamic $\sigma_d$) was calculated by equation 4.

$$\sigma_s(\sigma_d) = \frac{\mu_a - \mu_w}{\mu_a + \mu_w} \times 100\% \qquad (4)$$

Where $\mu_a$ and $\mu_w$ are the friction coefficients in the 'against-scale' and 'with-scale' directions, respectively.

**S2. The results of the tensile testing of the untreated, $TiO_2$ coated and N-doped $TiO_2$ coated wool fibers before and after irradiation**

**Table S1**. The results of tensile properties of wool fibers

| Irradiation time (h) | Untreated | | | | $TiO_2$ coated | | | | N-doped $TiO_2$ coated | | | |
|---|---|---|---|---|---|---|---|---|---|---|---|---|
| | Tenacity (MPa) | | Elongation (%) | | Tenacity (MPa) | | Elongation (%) | | Tenacity (MPa) | | Elongation (%) | |
| | Mean | SD | Mean | SD | Mean | SD | Mean | SD | Mean | SD | Mean | SD |
| 0 | 219 | 3.33 | 25.47 | 11.26 | 200 | 2.61 | 22.34 | 12.40 | 202 | 3.08 | 25.00 | 10.92 |
| 100 | 212 | 2.70 | 23.82 | 10.65 | 195 | 3.63 | 21.24 | 12.24 | 197 | 2.91 | 18.48 | 10.72 |
| 250 | 205 | 2.76 | 20.12 | 11.61 | 167 | 2.39 | 15.67 | 9.55 | 168 | 2.52 | 17.76 | 11.36 |
| 500 | 189 | 2.55 | 19.85 | 11.30 | 166 | 1.56 | 12.71 | 10.51 | 167 | 2.56 | 15.33 | 11.62 |

Note: Mean is denoted as the average value; SD is denoted as the standard deviation

## S3. The results of the friction testing of the wool fibers before and after treatments

**Table S2**. The results of friction properties of wool fibers

| Wool fibers | Friction coefficient | | | | Differential frictional coefficient (%) | |
|---|---|---|---|---|---|---|
| | Against-scale | | With-scale | | | |
| | Static | Dynamic | Static | Dynamic | Static | Dynamic |
| Untreated | 0.48 | 0.27 | 0.27 | 0.21 | 28.0 | 12.5 |
| $TiO_2$ coated | 0.53 | 0.39 | 0.35 | 0.31 | 20.5 | 11.4 |
| N-doped $TiO_2$ coated | 0.54 | 0.38 | 0.34 | 0.30 | 22.7 | 11.8 |

## S4. FESEM images of the wool fibers before and after treatments

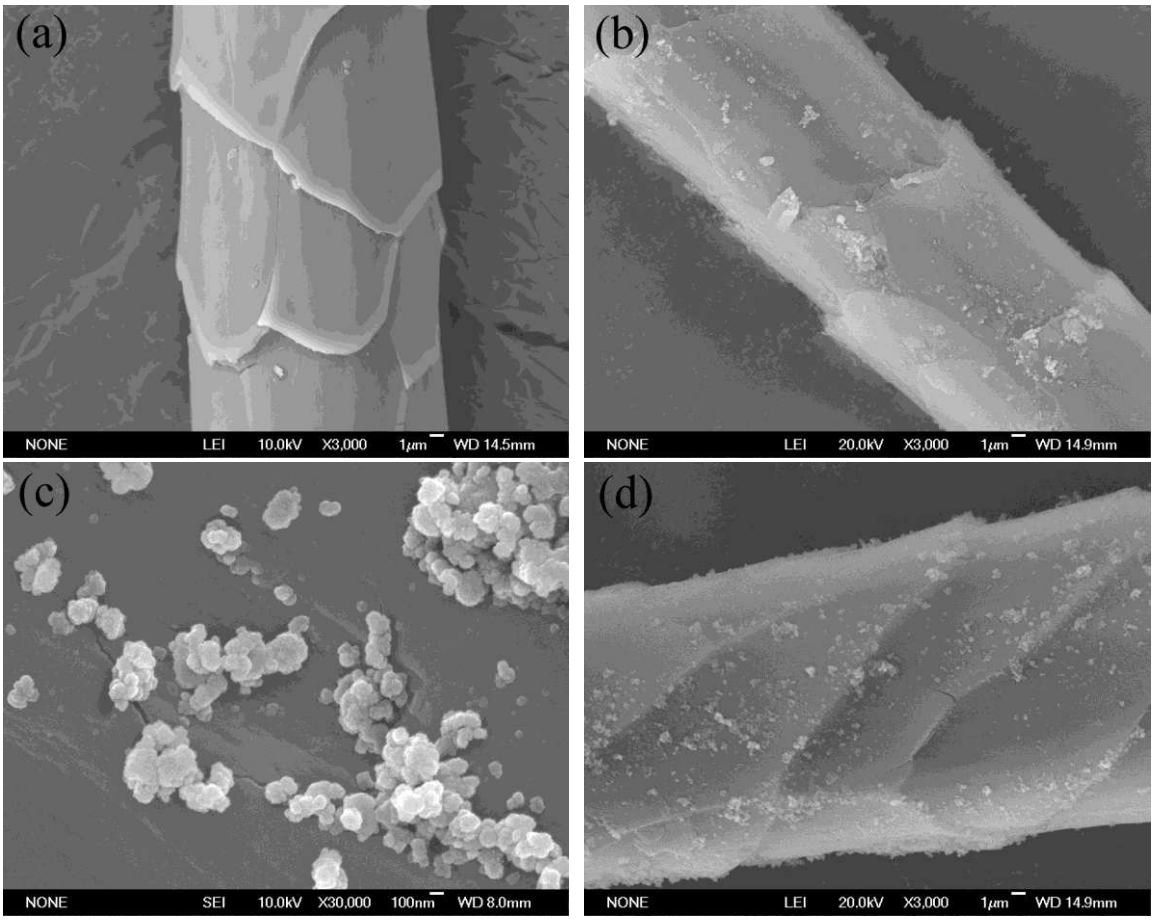

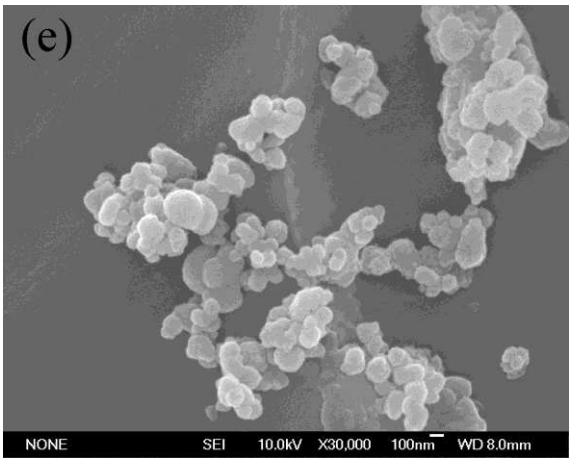


**Figure S1**. FESEM images of (a) 3000× untreated, (b) 3000× and (c) 30000× $TiO_2$ coated, and (d) 3000× and (e) 30000× N-doped $TiO_2$ coated wool fibers

## S5. The results of TG analysis of wool fibers

**Table S3.** The results of TG analysis of wool fibers

| Wool fibers | Onset decomposition temperature/°C | Endset decomposition temperature/°C | Decomposition rate /% |
|---|---|---|---|
| Untreated | 263.3 | 381.0 | 63.29 |
| $TiO_2$ coated | 259.7 | 370.7 | 67.03 |
| N-doped $TiO_2$ coated | 261.9 | 372.8 | 70.69 |

## S6. XPS spectra and core level single spectra of the bonding partners ($C_{1s}$, $O_{1s}$, $S_{2p}$, $N_{1s}$, and $Ti_{2p}$) of the wool fibers before and after treatments

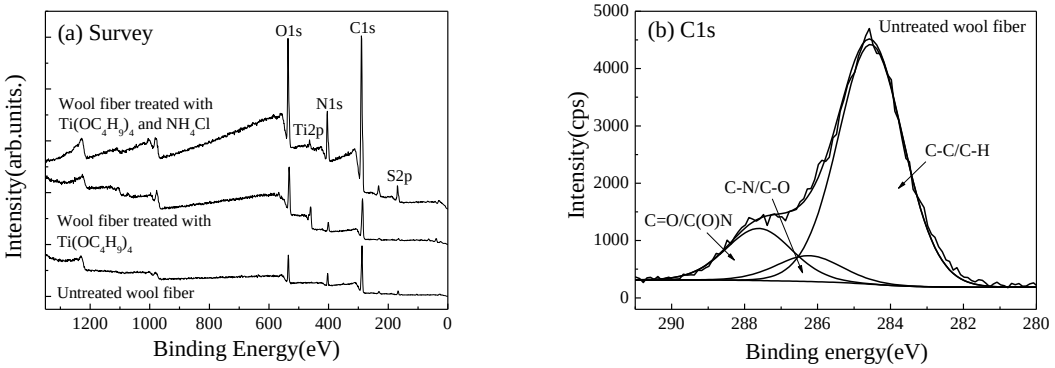

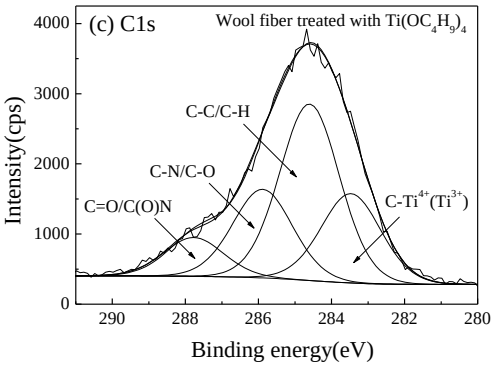
(c) C1s
Wool fiber treated with Ti(OC4H9)4
C-C/C-H
C-N/C-O
C=O/C(O)N
C-Ti4+(Ti3+)
Intensity(cps)
Binding energy(eV)

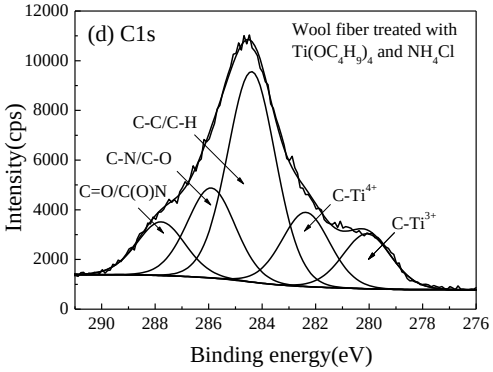
(d) C1s
Wool fiber treated with Ti(OC4H9)4 and NH4Cl
C-C/C-H
C-N/C-O
C=O/C(O)N
C-Ti4+
C-Ti3+
Intensity(cps)
Binding energy(eV)

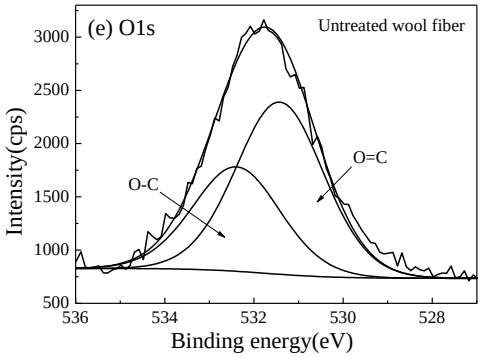
(e) O1s
Untreated wool fiber
O=C
O-C
Intensity(cps)
Binding energy(eV)

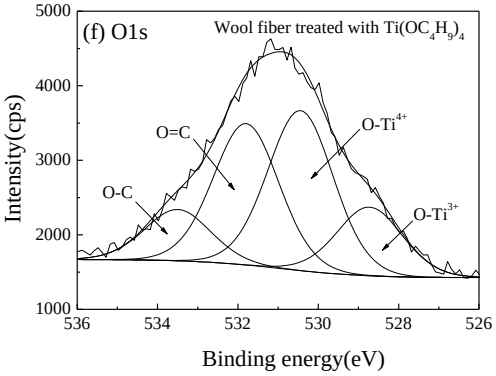
(f) O1s
Wool fiber treated with Ti(OC4H9)4
O=C
O-Ti4+
O-C
O-Ti3+
Intensity(cps)
Binding energy(eV)

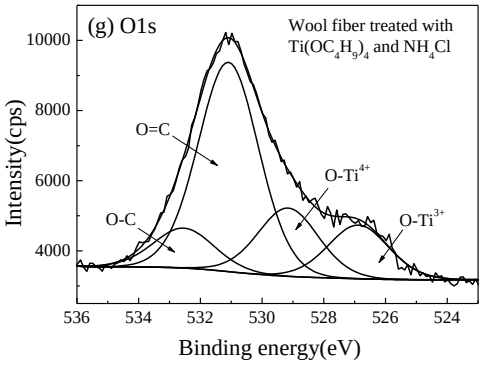
(g) O1s
Wool fiber treated with Ti(OC4H9)4 and NH4Cl
O=C
O-Ti4+
O-C
O-Ti3+
Intensity(cps)
Binding energy(eV)

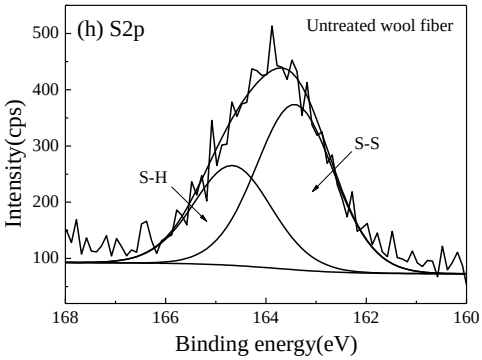
(h) S2p
Untreated wool fiber
S-S
S-H
Intensity(cps)
Binding energy(eV)

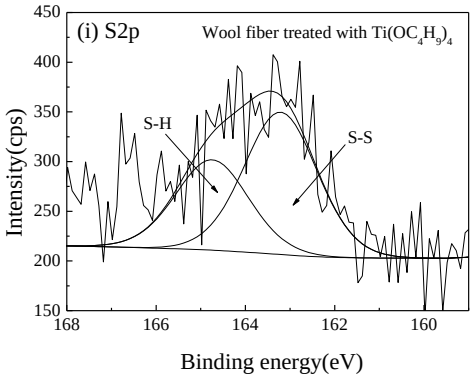
(i) S2p
Wool fiber treated with Ti(OC4H9)4
S-H
S-S
Intensity(cps)
Binding energy(eV)

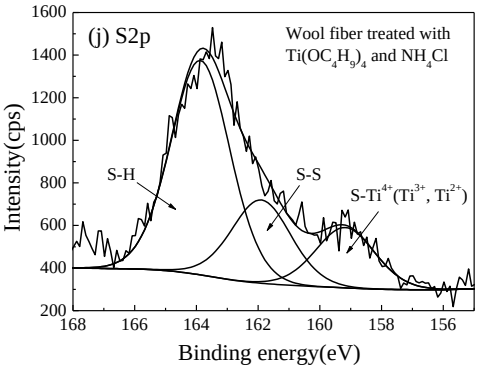
(j) S2p
Wool fiber treated with Ti(OC4H9)4 and NH4Cl
S-H
S-S
S-Ti4+(Ti3+, Ti2+)
Intensity(cps)
Binding energy(eV)

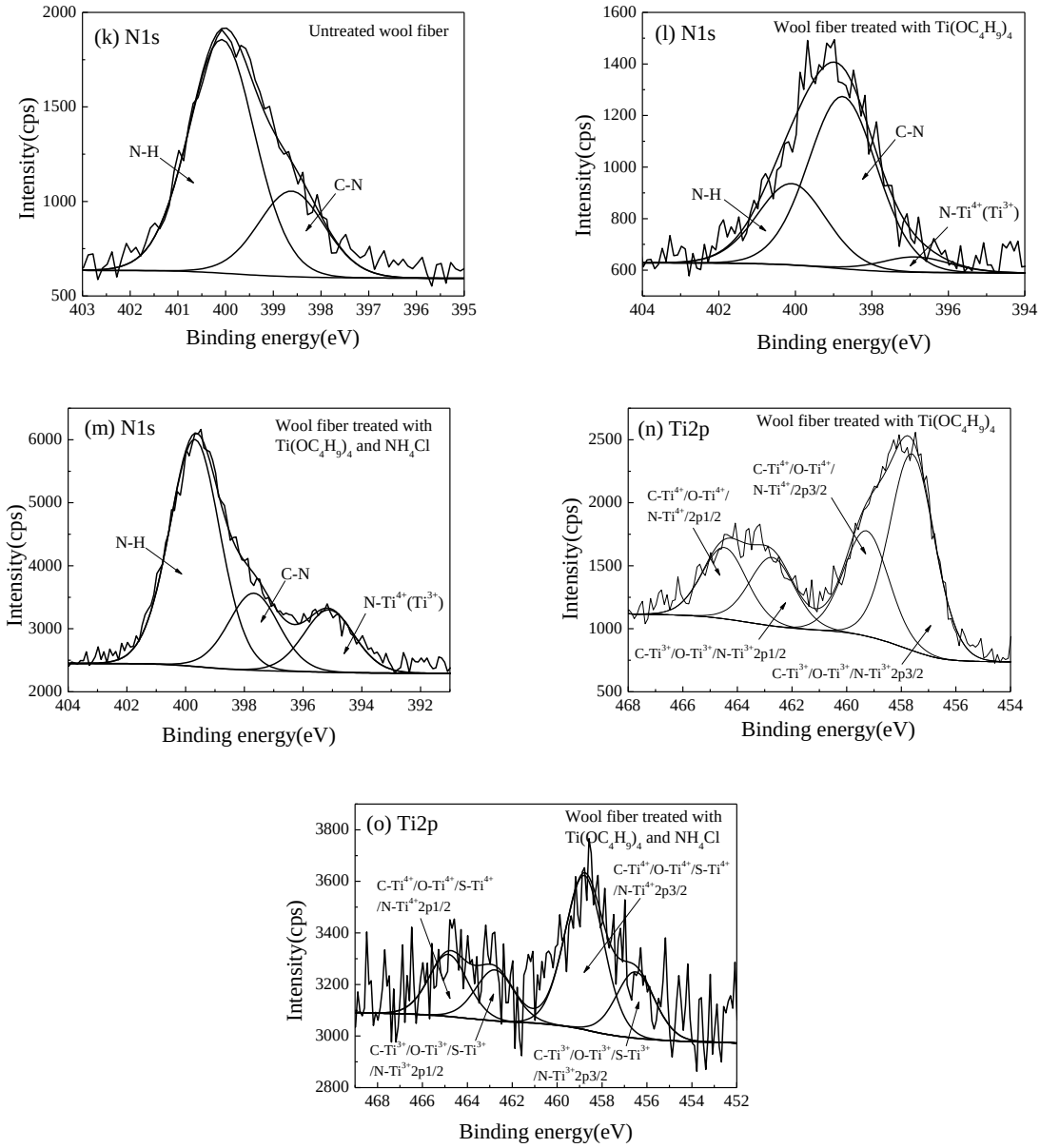


**Figure S2**. XPS spectra of wool fibers before and after treatments

(a) Survey spectra; (b) before and after treatments with (c) $Ti(OC_4H_9)_4$ and (d) $Ti(OC_4H_9)_4$ and $NH_4Cl$ of $C_{1s}$ spectra; (e) before and after treatments with (f) $Ti(OC_4H_9)_4$ and (g) $Ti(OC_4H_9)_4$ and $NH_4Cl$ of $O_{1s}$ spectra; (h) before and after treatments with (i) $Ti(OC_4H_9)_4$ and (j) $Ti(OC_4H_9)_4$ and $NH_4Cl$ of $S_{2p}$ spectra; (k) before and after treatments with (l) $Ti(OC_4H_9)_4$ and (m) $Ti(OC_4H_9)_4$ and $NH_4Cl$ of $N_{1s}$ spectra; after treatments with (n) $Ti(OC_4H_9)_4$ and (o) $Ti(OC_4H_9)_4$ and $NH_4Cl$ of $Ti_{2p}$ spectra

## S7. The quantitative XPS data

**Table S4.** XPS data of wool fibers before and after treatments

| Wool fibers | Peak | Binding energy/eV | FWHM/eV | Area/CPS.eV | Atomic concentration/% |
|---|---|---|---|---|---|
| Untreated | $C_{1s}$ | 284.57 | 2.37 | 12887.12 | 70.15 |
| | $N_{1s}$ | 399.91 | 2.04 | 3560.47 | 11.44 |
| | $O_{1s}$ | 531.80 | 2.56 | 6915.16 | 14.75 |
| | $S_{2p}$ | 163.84 | 2.29 | 1191.45 | 3.66 |
| $TiO_2$ coated | $C_{1s}$ | 284.59 | 2.99 | 11954.8 | 60.38 |
| | $N_{1s}$ | 399.15 | 2.62 | 2599.61 | 7.75 |
| | $O_{1s}$ | 530.98 | 3.56 | 11889.14 | 23.52 |
| | $S_{2p}$ | 163.54 | 2.95 | 962.46 | 2.74 |
| | $Ti_{2p}$ | 457.89 | 2.94 | 7997.36 | 5.61 |
| N-doped $TiO_2$ coated | $C_{1s}$ | 284.58 | 3.55 | 44648.40 | 67.29 |
| | $N_{1s}$ | 399.52 | 2.50 | 13790.28 | 12.26 |
| | $O_{1s}$ | 531.07 | 2.84 | 26431.49 | 15.61 |
| | $S_{2p}$ | 163.51 | 2.87 | 4633.59 | 3.95 |
| | $Ti_{2p}$ | 458.61 | 1.69 | 4261.93 | 0.89 |

## S8. PL spectra of the wool fibers before and after treatments

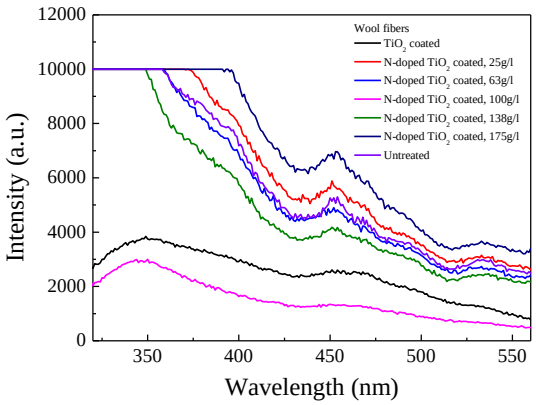


**Figure S3**. PL spectra of wool fibers before and after treatments

## S9. The change of normalized $C_0/C$ of MB concentration for the untreated, $TiO_2$ coated and N-doped $TiO_2$ coated wool fibers with irradiation time under UV or visible light irradiation

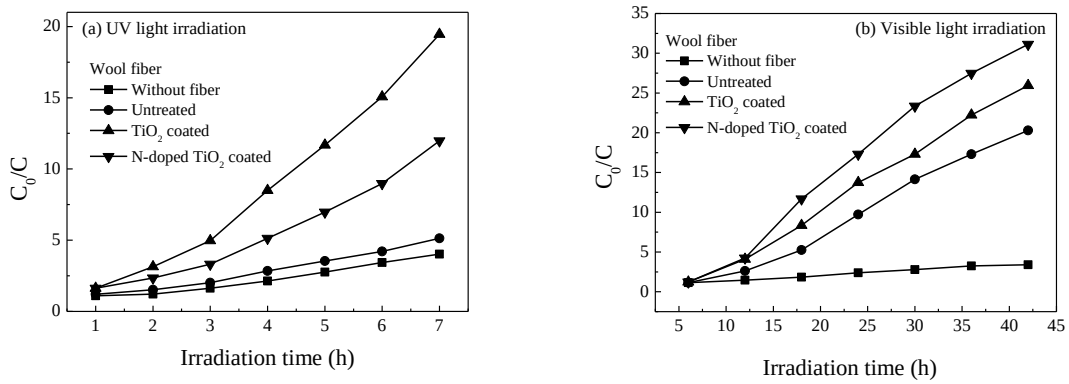


**Figure S4**. Variation of normalized $C_0/C$ of MB concentration as a function of irradiation time: (a) UV light and (b) visible light irradiation

**Supporting References**

[S1] H. Zhang, X. Zhang, X. Yang, Facile Synthesis of Monodisperse Polymer/$SiO_2$/polymer/$TiO_2$ Tetra-layer Microspheres and the Corresponding Double-walled Hollow $SiO_2/TiO_2$ Microspheres. *J. Colloid Interf. Sci*. **348** (2010) 431–440.

[S2] L. Segal, J. J. Creely, A. E. Martin Jr., C. M. Conrad, An Empirical Method for Estimating the Degree of Crystallinity of Native Cellulose Using the X-ray Diffractomer. *Text. Res. J*. **29** (1959) 786−794.

[S3] F. X. Ye, T. Tsumura, K. Nakata, A. Ohmori, Dependence of Photocatalytic Activity on the Compositions and Photo–absorption of Functional $TiO_2$–$Fe_3O_4$ Coatings Deposited by Plasma Spray. *Mater. Sci. Eng. B–Adv.* **148** (2008) 154–161.

[S4] M. Lipson, P. Howard, Friction between Keratin Surfaces as Affected by Some Shrinkproofing Treatments. *J. Soc. Dyers Colour*. **62** (1946) 29−32.

[S5] M. Mori, N. Inagaki, Relationship between Anti-felting Properties and Physicochemical Properties of Wool Fibers Treated with Ar-plasma. *Tex. Res. J*. **79** (2006) 687–694.